Brazilian Journal of Chemical Engineering (2023) 40:1067–1076
https://doi.org/10.1007/s43153-022-00297-5

ORIGINAL PAPER

Thermally induced nano-texturing of natural materials: *Mytilus galloprovincialis*, *Mya arenaria* and *Cerastoderma edule* exoskeletons

Alexandra I. Bucur[1] · Maria Poienar[1] · Raul A. Bucur[1] · Cristina Mosoarca[1] · Radu Banica[1]

Received: 31 August 2022 / Revised: 16 December 2022 / Accepted: 21 December 2022 / Published online: 9 January 2023

Abstract

Sea shells exoskeletons are an important source of calcium carbonate and trace elements, being suitable for many applications in agriculture, constructions, chemical and furniture industry, wastewater treatment, lime production etc. This paper presents a study of the structure, composition, thermal behavior and surface thermal texturing of *Mytilus galloprovincialis*, *Mya arenaria* and *Cerastoderma edule* shells from the Black Sea. XRD results revealed differences in the crystalline composition depending on the species (under certain conditions representing an imprint of the species to which they belong and place of origin). Aragonite of biogenic origin begins to decompose to calcite at a temperature below 250 °C. The rate of decomposition appears to be influenced by the biological species of origin. $CaCO_3$ content was established by chemical analysis and microstructure details were revealed by SEM analysis. A new material based on marine exoskeletons was obtained by short-time heat treatment of exoskeletons around a temperature of 700 °C, leading to the formation of a material with specific porosity—ordered and with narrow dimensional distribution, which is related to the initial structure of the exoskeletons. The superficial modification of exoskeletons by heat treatment leads to an increase of the surface reactivity, without altering the natural hierarchical structure. Potential applications of these textured shells include anchoring bacteria (biomass growth on natural supports) for biofiltration processes or reactive natural template for the synthesis of inorganic nanotubes.

Keywords Marine exoskeletons · Surface texturing · Calcium carbonate · Exoskeletons decomposition · Natural materials

Introduction

The increased need for food because of population rise leads to problems such as microbial decomposition of wastes and production of harmful compounds (Silva et al. 2019). Many tons of shells exoskeletons from food processors are dumped every year as waste (Summa et al. 2022), with examples such as the canning industry in Galicia, which produces 25,000 tonnes of mussel by-product/year (unconsumed shells) (Martínez-García et al. 2020) or the production of 309,886 tons/year of green mussels in Indonesia (data in 2018), leading to 216,902 tons of waste of green mussel shells (Ismail et al. 2021). In the meantime, much smaller amounts of shells waste have found usage in different applications, such as partial cement replacement and concrete aggregates, ceramic and plastic additives, biofilter medium, biomedical applications, artificial stones and many more (Hart 2020; Lin et al. 2022; Silva et al. 2019; Wan Mohammad et al. 2017). Calcium carbonate from shells may be a natural alternative to calcium carbonate from mined limestone in the composite materials production (Owuamanam and Cree 2020) or wastewater treatment (Jones et al. 2011). Since shells are very abundant in nature and their exoskeletons may represent an ecological cheap alternative to more expensive or less environmentally friendly materials currently in use, their potential should be further investigated. For example, an energy-saving way to integrate shells waste by transforming them into useful construction materials was recently proposed (Bucur et al. 2022).

Best solutions for materials applications require renewable, natural and cheap resources, which shells are. The interesting aspect is the shells inner structure, which for most mollusks is composed of one organic layer and two to five calcified inorganic layers (Marin et al. 2012). The outer organic layer is the *periostracum*, then there is the *prismatic layer* and the *nacre*—both composed of calcium

✉ Radu Banica
radu.banica@yahoo.com

[1] National Institute for Research-Development in Electrochemistry and Condensed Matter, No. 144 Dr. Aurel Paunescu Podeanu, 300569 Timisoara, Romania

carbonate crystals (Harayashiki et al. 2020). Together with the biopolymers between them [containing polysaccharides i.e. chitosan, glycosaminoglycans, polypeptides, proteins, nucleic acids, etc. (Agbaje et al. 2021; Ruiz-Hitzky et al. 2005)], the inorganic layers form nano-biocomposites, structures that offer a wide range of functional properties.

The calcium carbonate, which accounts for minimum 95% of the shells composition (Harayashiki et al. 2020), crystallizes in more forms (called polymorphs). The first two most spread polymorphs in shells are calcite and aragonite (Wang et al. 2014), present in different proportions in the prismatic layer (for some shells, only one of them forms the prismatic layer), depending on the shell species and other factors. In most cases, the prismatic layer is composed of elongated crystals (but obliquely positioned crystals can also be found), placed perpendicularly to the shell surface, while the nacreous layer crystals are arranged in the form of flat units parallel to each other (Marin et al. 2012) and generally (but not necessarily) parallel to the outer surface of the shell. The nacre lamellae are always made of aragonite (Marin et al. 2012). Flat tablets of aragonite in the nacreous layer are a few micrometers wide and have thicknesses in the submicrometric domain (Marin et al. 2012), while the protein layers that bind the mineral lamellae have thicknesses of tens of nanometers (Ruiz-Hitzky et al. 2005). The aragonite tablets are interconnected by bridges formed within pores that cross the organic layer (Schäffer et al. 1997). The biological carbonate fibers form a perfectly stacked structure, with "stacks twisted in a plywood-like arrangement" (Roda et al. 2019). Such stacked structures of inorganic crystals and biopolymers possess remarkable mechanical properties (Marin et al. 2012; Ruiz-Hitzky et al. 2005). Interestingly, although aragonite is a metastable form of calcium carbonate (Owuamanam and Cree 2020), it is encountered in many shells, forming well-defined structures. A wide variety of crystal habits are used by mollusks, and especially bivalves, to construct their shells structure; therefore, the common terminology for these shell habit groups is "shell microstructure" (Marin et al. 2012). The knowledge of the microstructure determines, for example, the knowledge of the biomechanical behavior (Connors et al. 2012) or of other characteristics, that could determine the appearance of bio-inspired applications. Examples go from bone analogues for tissue engineering made of corals (Ben-Nissan 2003) to composites in the shape of hydrogel beads of copper-doped *Cerastoderma edule* used for pesticides removal from water (Aziz et al. 2023). Mussel shells were found to have thermal and acoustic properties that make them suitable for using as building insulation materials (Martínez-García et al. 2020). They are also efficient for nitrate (Abali et al. 2021; Von Ahnen et al. 2018) or phosphate (Tran et al. 2021) removal from effluents. Although much effort has been put into studying the inorganic matrix, Ehrlich et al. (2020) recently proposed an isolation method for the organic scaffold, that preserves the initial shape and size of the exoskeletons, for applications such as biomedicine, cosmetics, pharmacy etc. The cement companies apply bio-inspired methods for atmospheric CO_2 sequestration (Morris et al. 2016).

Thermal treatment of shells is a common method used in the assessment of the thermal stability of these materials (Li et al. 2015), or as a method to use the shells as calcium carbonate source, by transforming the latter into oxide (complete transformation of shells). The transformation of aragonite to calcite starts at a temperature of approximately 280 °C (Yoshioka and Kitano 1985), while at a temperature as high as 900 °C the calcite is already completely transformed into calcium oxide (Silva et al. 2019). Thermal treatment with complete transformation of carbonate leads to a friable material, with complete loss of shape and destruction of the structural order that is naturally present in shells (Li et al. 2015).

Partial thermal decomposition has not been the subject of many studies. Recent findings show that the thermal treatment of 15 min at 300 °C adjust the organic matrix/aragonite interface bonding, but the result is species-dependent (Li et al. 2022). Pap et al. (2022) activated mussel and oyster shells for phosphate removal by heating them to 700 °C for 1 h and obtained higher phosphate removal efficiency compared to raw shells. Good phosphate removal efficiency was also obtained by using pretreated shells (at 400 °C for 0.5 h, at 400 °C for 2 h and 700 °C for 2 h) (Tran et al. 2021).

In this paper we propose a new, promising approach, by making use of thermal treatment as a *functionalization method* for the exoskeletons surface. The heating of the shells to high temperatures for short time allows the decomposition of just a small percentage of carbonate. If only the surface is textured, then most of the mechanical properties and the original shape of the convex valves of shells will be preserved, while the surface reactivity should increase. These textured materials will be used in a future project as water biofiltration substrates, so maintaining the structural integrity is compulsory. The modification of the surface topography was carried out in order to obtain the attachment centers for the bacterial biofilm and hopefully to improve the chemosorption properties. This concept, of surface texturing, is new and has not been proposed anywhere in the literature, to our knowledge.

Experimental

Identification

A few kg of mollusk shells were collected from the Black Sea shores (Mangalia region) and examined by a biologist to determine their species. Of all the present species, *Mytilus*

galloprovincialis (MG), *Mya arenaria* (MA) and *Cerastoderma edule* (CE) have been separated. These were predominant in the collected quantity and have been previously identified by other authors (Hart 2020) as being widespread along the Black Sea coast.

Processing

Three powder samples were prepared for physico-chemical characterization using these shell types: *Mytilus galloprovincialis, Mya arenaria and Cerastoderma edule* (samples called MG, MA and CE). The exoskeletons of each type were ultrasonicated in distilled water at room temperature, then the water was drained and the washing was repeated for a number of times under ultrasound treatment with fresh amounts of water. After the final rinsing followed by drying for 2 h at 80 °C, the shells were broken, using the hydraulic press, under 5 tons force pressure for 30 s. Afterwards, the shells were sieved through sieves of different mesh sizes and the fraction < 200 µm was considered for this study. Based on preliminary thermal analysis results, further thermal treatment studies envisaged a deeper understanding of the influence of heat treatment on the structure and composition of marine exoskeletons. Thermal processing was acquired by heating each sample of < 200 µm particles size in a preheated furnace, in glazed crucibles, at a specified temperature (250, 300, 350, 400 and 450 °C) for 1 h. After cooling to room temperature, each sample was analyzed by XRD, the resulting samples being named MG250–450, MA250–450 and CE250–450.

High temperature texturing implied the heating of each sample to a high temperature (600, 700 and 800 °C) for a short period of time (180 s). Each sample consisted in 5 g mixed exoskeletons fragments of the fraction 4–7 mm. In all cases the samples were placed in the preheated oven at working temperature, on a metal mesh with thin stainless steel wires and very low thermal inertia. The resulting samples are named MX600, MX700 and MX800. After the thermal treatment, the samples were extracted and cooled during 3–4 min to temperatures below 100 °C, afterwards being closed in sealed containers. For the SEM analysis, the samples were broken using tweezers in order to visualize their sections. The marks in the SEM images, the angles and the voids dimensions were determined using the ImageJ free software (Schneider et al. 2012).

Physico-chemical characterization

X-Ray powder diffraction patterns were obtained using an X'Pert PRO MPD diffractometer with PixCEL detector and copper anode (λ = 1.5406 Å), working parameters: 45 kV and 30 mA, step size 0.01 Å, 2θ domain = 20°–70°.

The morphology of the obtained powder specimens was studied by Scanning Electron Microscopy (SEM) using an electronic microscope Model Inspect S (FEI Company) coupled with an EDS detector. Working parameters are: low vacuum, spot size 2.5–3, working distance 10–12 mm. Semi-quantitative analysis of shell samples was performed using the energy-dispersive X-ray spectroscopy (EDS). The crystal structures of the two polymorphs were visualized using the Vesta software (Momma and Izumi 2011).

The $CaCO_3$ content (% mass) was established by titration of the Ca^{2+} ions with a 0.025 M Na_2EDTA solution at pH = 9.8 ± 0.3 (using NH_3/NH_4Cl buffer) in the presence of Eriochrome Black T/KCl as indicator at room temperature. The total concentration of the CO_3^{2-} ions in the exoskeletons was determined by measurement of the evolved CO_2 during hot HCl dissolution, for desorption of the dissolved CO_2.

Thermal stability was studied using the SETARAM Lab Sys Evo equipment. The powder (< 200 µm) was placed in alumina crucibles and heated with 15 °/min heating rate in synthetic air (42 mL/min), up to 1000 °C.

Results and discussion

The aragonite is a meta-stable allotropic modification of $CaCO_3$ with often fibrous or columnar growth (Marin et al. 2012), and hardness higher than calcite (Troncoso et al. 2020). The aragonite structure was first determined by W. L. Bragg in 1924 (Bragg and Langworthy 1924) and more recently high-resolution synchrotron powder diffraction measurements confirmed its orthorhombic symmetry (space group Pmcn) (Caspi et al. 2005), where the Ca (blue color) site is nine-fold coordinated by O (red color), as shown in Fig. 1. The carbon (depicted in brown color) lies at the center of the triangle formed by the three oxygens at each corner, each CO_3 group stands between six Ca atoms and lies in two planes that point in opposite directions, while in calcite structure the carbonate ions lie in a single plane pointing in the same direction. Aragonite is thermodynamically metastable, with a tendency to transform into calcite, which is the stable form (Marin et al. 2012). This transformation is accelerated by the temperature increase. The oriented crystalline growth of aragonite is possible to improve the exoskeletons mechanical resistance. The rhombohedral crystal structure of calcite was first determined using X-ray diffraction (XRD) by Bragg in 1914, and can be expressed by using the hexagonal settings (Ishizawa et al. 2013). In the calcite structure, the Ca cation (blue color, in Fig. 1 right) is surrounded by six oxygen atoms (red color) in a regular octahedron (Ca–O distance X6 = 2.3627 Å). Consequently, the calcite structure is a layered crystalline structure formed by alternating layers of CO_3^{2-} groups and Ca^{2+} ions. The crystalline structure of aragonite thus differs from the calcite

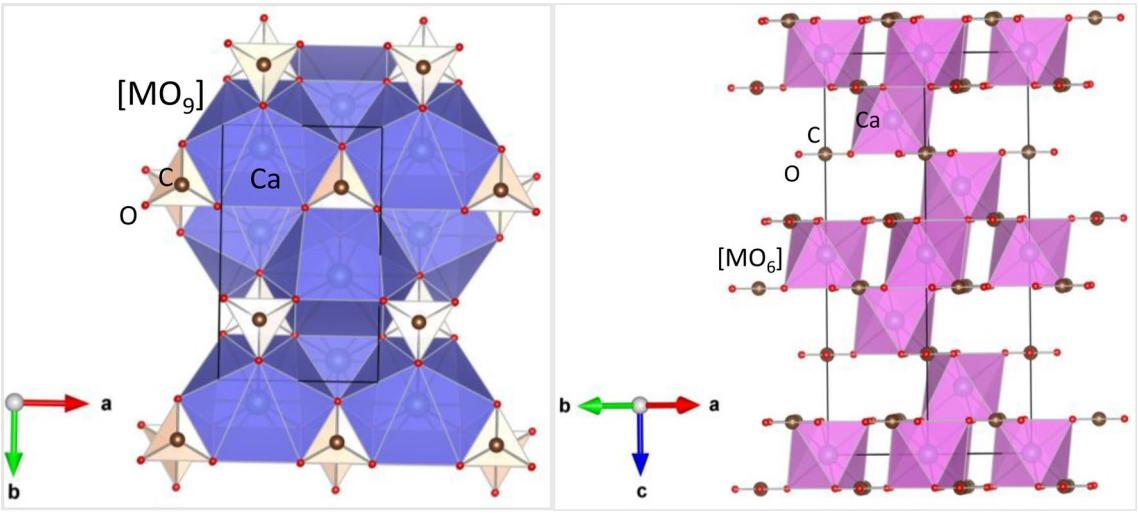

Fig. 1 The aragonite type crystal structure (space group Pmcn)—left, and the calcite type crystal structure (space group R-3 c)—right

one as the coordination number for the cations in the calcite is [MO_6] and in the aragonite network is [MO_9], and also the CO_3^{2-} groups are arranged differently in calcite and aragonite phases. Moreover, each oxygen atom in CO_3^{2-} group is surrounded by two Ca^{2+} ions in the calcite and three in aragonite (Bragg and Langworthy 1924).

The XRD patterns of the three shell samples are presented in Fig. 2a. For the original, not heat-treated samples, patterns indicate that these are well-crystallized, as the peaks are narrow and clearly defined. From the comparison of the three specimens, it can be observed that MG presents supplementary peaks compared with samples 2 and 3.

The identification revealed the existence of aragonite and calcite (two polymorphs of calcium carbonate) in the MG sample, and only aragonite in the MA and CE samples. The characteristic peaks of aragonite structure were indexed according to ICDD File No. 01-076-0606, while the supplementary peaks from MG (Fig. 2) are associated to calcite polymorph based on the ICDD File No. 01-085-1108 (Kamba et al. 2013).

The biogenic aragonite grows oriented along the crystalline plane (012), as XRD shows, but there is a big difference between the oriented growths of the three species. In the case of the CE species, the growth oriented along the plane (012) is much stronger than in the case of the MA sample, which in turn shows a preferential growth in this direction stronger than the MG sample. This oriented growth is probably due to the weaker adsorption of the proteins synthesized in the mollusk on the crystalline plane (012) than on the competing planes, which allows the growth in this direction [phenomenon called "geometrical selection" (Saruwatari et al. 2009)].

The heat treatment at various temperatures highlights the complete transformation of aragonite into calcite up to the

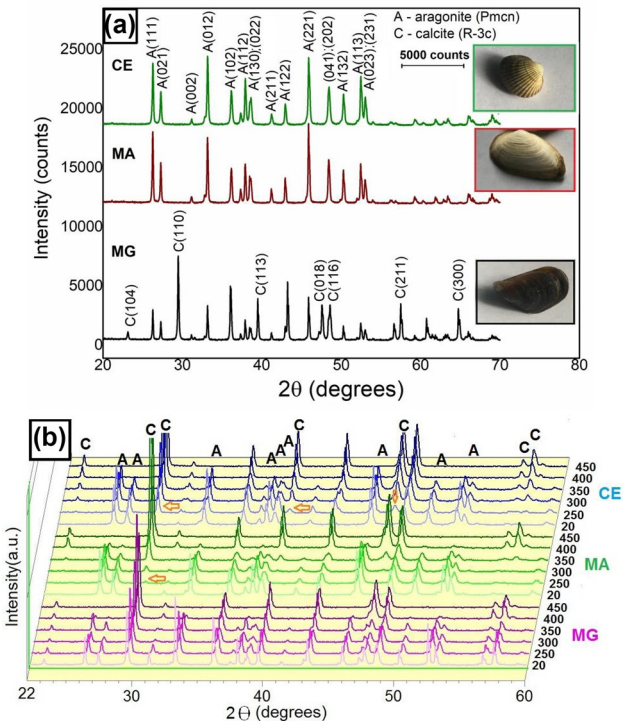

Fig. 2 **a** XRD patterns of the fraction containing particles < 200 µm for: MG, *Mytilus galloprovincialis*; MA, *Mya arenaria*; CE, *Cerastoderma edule*. The peaks corresponding to each phase are denoted by C for calcite, respectively A for aragonite. For a better visualization, the intensity values for MA and CE samples have been shifted with respect to the initial values (with 10,500 for MA and 16,000 for CE), **b** XRD patterns of the fraction containing particles < 200 µm for MG, MA and CE after thermal treatment for 1 h at different temperatures (values are in °C)

temperature of 450 °C in the case of MG and MA samples and up to 400 °C in the case of the CE sample (Fig. 2b). The heat treatment at 250 °C produces only a beginning of an allotropic transformation for the MG and MA samples, highlighted by the presence of the (110) peak of the calcite (the calcite's most intense peak). At the same temperature in the case of the CE sample, the allotropic transformation is already significant, the (110), (113) and (116) peaks of the calcite being clearly observable in the XRD spectrum. Therefore, the *species* of mollusk influences the thermal behavior of aragonite in the structure of exoskeletons.

The atomic positions and space group (Bragg and Langworthy 1924; Caspi et al. 2005; Ishizawa et al. 2013), along with the unit cell parameters extracted from Rietveld refinement performed with the FullProf Software (Rodríguez-Carvajal 1993) for the three samples, are presented in Table 1.

Due to the complex crystal growth of these exoskeletons with the intercalation of organic molecules within the inorganic crystallites, numerous defects appeared at the nanoscale level of the structures, which justify the strain used in the refinement of the biogenic aragonite crystalline structure (Pokroy et al. 2007). These structural stresses could be at the origin of some oriented growth phenomena present in the studied shells samples. The increase of temperature up to 200 °C induce more strain fields, probably associated with different oriented and intercalated domains of organic/inorganic layers, dislocations etc.

Figure 3 presents the cross-section SEM images for three pieces belonging to the studied types of shells. The exoskeletons of the MG species are composed of periostracum (top), prismatic (middle) and nacre (bottom) layer (Harayashiki et al. 2020). The nacreous layer is very thin and contains sheets parallel to the outer surface, while the prismatic layer accounts for more than 80% of thickness for the studied piece of shell. This contains obliquely (relative to the outer surface of the shell and parallel to the yellow arrow) disposed needle-like crystals, as can be seen in Fig. 3a. At higher magnification it is observable that this structure is composed of parallel columnar fibers with high shape coefficient and lengths of tens of microns (Fig. 3a inset). Cross-section image of MA (Fig. 3b inset) highlights hardly discernable layers of very thin short needle-like crystals, with spongy-bone general aspect.

The cross-section images for the CE sample highlight a completely different structure. It can be seen that the total thickness of the studied exoskeleton piece is significantly higher than in the case of the other samples (for pieces of similar weight), reaching in some places over 1 mm (Fig. 3c). At higher magnification, a complex crossed lamellar structure is observed, where a plywood appearance is clearly visible (Fig. 3c inset). The crystalline braid is made up of large crystalline beams that are superstructures made of crystalline fibers (parallel to the yellow lines), with diameters of tens or hundreds of nanometers and multi-micrometric lengths. These large superstructures intertwine at almost right angles, of approx. 104°, as can be seen in Fig. 3c—inset. The MG shell present, therefore, a clearer and well-defined inner structure, compared to the samples containing the single phase aragonite, and the prismatic layer is thicker.

Table 1 The space group, atom parameters and the calculated unit cell parameters from Rietveld refinement for MG, *Mytilus galloprovincialis*; MA, *Mya arenaria*; CE, *Cerastoderma edule*

MG		
Phase	Aragonite	Calcite
Space group	P m c n (No. 62)	R −3 c (No. 167)
Atom parameters	Ca 0.25 0.41502 0.75985 C 0.25 0.76194 −0.08240 O1 0.25 0.92238 −0.09453 O2 0.47499 0.68012 −0.08725	Ca 0 0 0 C 0 0 0.25 O 0.25530 0 0.25
Unit cell parameters	$a=4.9641(2)$ Å, $b=7.9630(4)$ Å, $c=5.7496(3)$ Å, $\alpha=\beta=\gamma=90°$; *Vol*: 227.280 (2) Å^3	$a=b=4.9852$ (2) Å, $c=17.0527(8)$ Å, $\alpha=\beta=90°$, $\gamma=120°$; Vol: 367.015 (3) Å^3
MA		CE
Phase	Aragonite	Aragonite
Space group	P m c n (No. 62)	P m c n (No. 62)
Atom parameters	Ca 0.25 0.41502 0.75985 C 0.25 0.76194 −0.08240 O1 0.25 0.92238 −0.09453 O2 0.47499 0.68012 −0.08725	Ca 0.25 0.41502 0.75985 C 0.25 0.76194 −0.08240 O1 0.25 0.92238 −0.09453 O2 0.47499 0.68012 −0.08725
Unit cell parameters	$a=4.9642$ (2) Å, $b=7.9615$ (2) Å, $c=5.74942$ (1) Å, $\alpha=\beta=\gamma=90°$; *Vol*: 227.228 (1) Å^3	$a=4.9631(2)$ Å, $b=7.9626$ (3) Å, $c=5.74895$ (2) Å, $\alpha=\beta=\gamma=90°$; *Vol*: 227.190 (1) Å^3

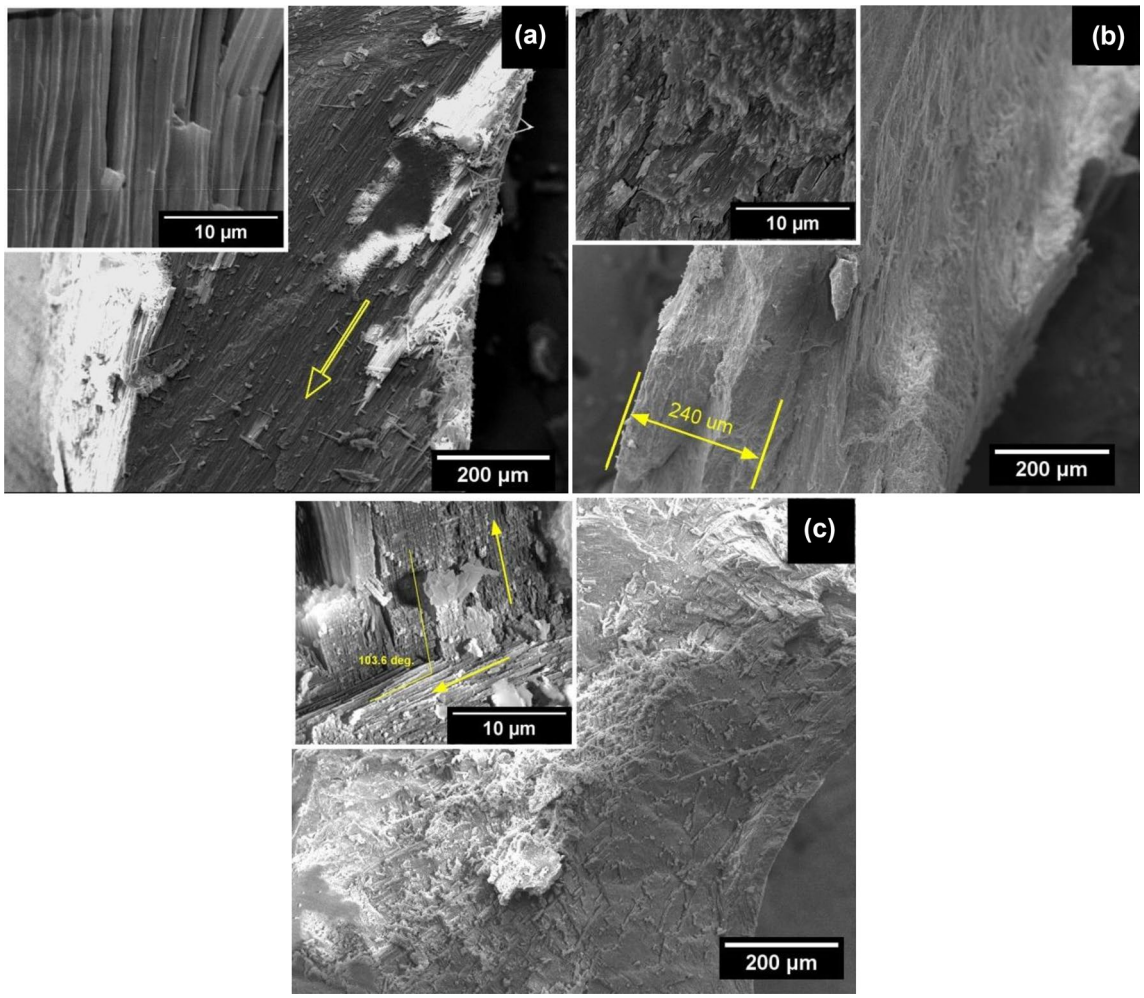

Fig. 3 Cross-section SEM images for **a**—MG, **b**—MA and **c**—CE samples

EDS patterns (not presented) have confirmed the presence of carbon at 0.28 keV, oxygen (0.53 keV), calcium (3.69 keV) and some trace elements.

The chemical analysis based on the titration of Ca^{2+} ions revealed a concentration of 97.9 wt% $CaCO_3$ for MG and 98.6 wt% for MA and CE samples. The determination error for the considered volumes is of maximum 1.5%. This analysis is in good agreement with the volume of CO_2 determined both by acid dissolution and by thermal decomposition, as will be seen from the TG analysis. Thus we can conclude that in all cases the exoskeletons are formed of $CaCO_3$ in a weight concentration of over 96%.

The overall TG analysis is presented in Fig. 4a and a detail in the range 25–500 °C is shown in Fig. 4b. For all samples, two mass losses can be highlighted: the first, less than about 1.2–1.3% in the temperature range 160–450 °C, and the second, of about 41%, in the temperature range 610–880 °C. The decomposition is accompanied in all cases by weak exothermic effects in the DTA spectrum, which start at 118 °C and 278 °C respectively for the MG sample, with maxima at about 152 °C and 339 °C. The later exothermic effect is clearly highlighted for the mentioned sample (MG), and is extended over a range between 240 and 550 °C for the other two samples.

Studying the details of this first decomposition, presented in Fig. 4b-inset, one can say that at a temperature below 200 °C the exothermic effect may be due to reactions associated with folding, reaction (1)-see below, and denaturation of protein chains. Even in aqueous environment between 40 and 100 °C, the DSC studies have shown strong exothermic effects associated with protein chain packaging (Johnson 2013). The absence of water in the exoskeleton composition is expected to slow down these processes by reducing the mobility of protein chains and by the absence of hydrolysis reactions. At temperatures above 200 °C, exothermic reactions of protein oxidation according to reaction (2) and reactions of modification of the allotropic form of aragonite into calcite according to reaction (3) take place.

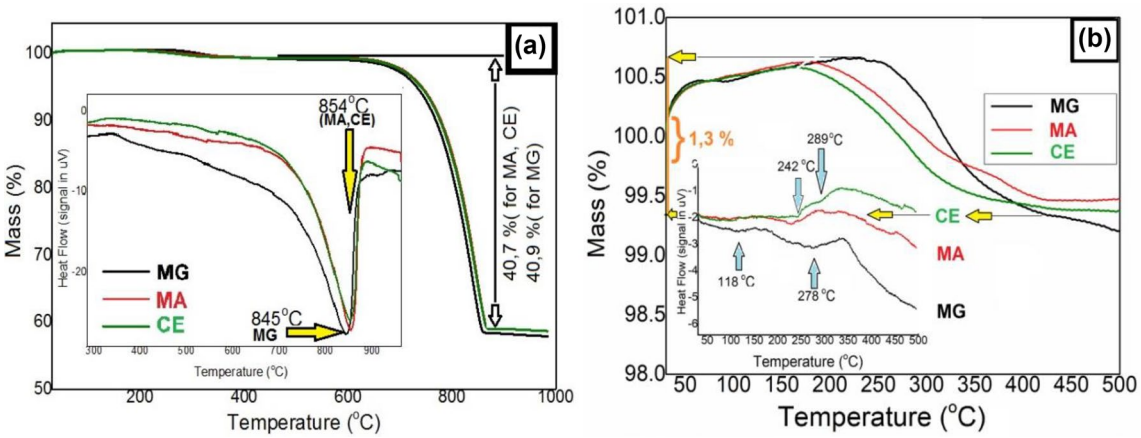

Fig. 4 Thermal analysis curves for MG, MA and CE, fraction < 200 µm, heating rate 15 °/min in air

In particular, in the case of the CE sample, the observed extended exothermic effect consists in two stages starting at 242 °C and 289 °C (Fig. 4b—inset). As can be seen in the XRD spectrum, Fig. 2b, the CE sample is the only one for which the significant transformation of aragonite into calcite takes place at a temperature lower than 250 °C. For this reason it is possible that the exothermic effect starting at 242 °C to be attributed to the superposition of 2 processes (An et al. 2013): the transformation of aragonite into calcite according to the reaction (3), which is an endothermic process, and the oxidative degradation of proteins, an exothermic effect, leading to the DTA curves presented in Fig. 4b. The presented data, as well as literature data, show that aragonite of biogenic nature has slightly different properties from sample to sample, depending on the particularities of the organism by which it was produced.

The oxidative process of organic matter is also exothermic and occurs at higher temperatures, being coupled with mass losses due to the loss of CO_2, H_2O and N_2, for the oxidation of amino groups. Oxidation is conditioned by the diffusion of oxygen through aragonite and calcite crystals. This explains the existence of the weak exothermic processes up to temperatures of about 550 °C, with over 100 °C higher for the MG and MA samples or 150 °C higher for the CE sample, than the temperature at which, according to the XRD spectra in Fig. 2b, there is no aragonite in the system.

The decomposition of calcite to calcium oxide according to reaction (4) begins for all samples in the temperature range 591–597 °C, being a strongly endothermic process (Jones et al. 2011; Kamba et al. 2013), having the minima at 854 °C (MA, CE sample) and 845 °C (MG sample) visible in Fig. 4a-inset. The calcite decomposition is complete for the MG sample at 865 °C and 874 °C for the other two samples, as seen in Fig. 4a.

$$\text{Exoskeleton} + Q \rightarrow \text{Exoskeleton (denaturated protein)} + H_2O;(T: RT - 200\ ^\circ C) \quad (1)$$

$$\text{Denat. proteins} + O_2 \rightarrow CO_2 + H_2O + \text{by-products} + Q;(T: 200 - 550\ ^\circ C) \quad (2)$$

$$CaCO_3(\text{aragonite}) + Q \rightarrow CaCO_3(\text{calcite});(< 250 - 450\ ^\circ C) \quad (3)$$

$$CaCO_3(\text{calcite}) + Q \rightarrow CaO + CO_2;(591 - 874^\circ C). \quad (4)$$

Shells are promising for water purification applications, for example as phosphate removal absorbents, and thermal treatment may improve this property. Pap et al. (2022) activated the shells for phosphate removal by heating them to 700 °C for 1 h. Waste of mussel shells showed high efficiency of zinc removal from surface runoff, with thermal treatment of 15 min at 500 °C improving this ability (Odeh et al. 2022). Organic matter removal from shells was applied in order to increase the exoskeleton's exposure to runoff and to prevent the future growth of organic matter onto shells (Odeh et al. 2022). Common thermal treatment implied the heating of shells to temperatures of maximum 500 °C for no more than 2 h, with a standard method proposed by Barros et al. (2009)—of 500 °C for 15 min.

We propose a method to texture the surface of the mollusk exoskeletons, by heat treatment for short times at high temperatures. Since the required time in order to texture the shells surface is of few minutes, the economic implications of such a method are lower that processing the shells for a few hours at high temperature (Morris et al. 2016). Based on the presented thermogravimetry results, where it can be seen that around 597 °C the decomposition

of calcium carbonate starts, the temperatures of 600, 700 and 800 °C were chosen for tests for MX samples series. Weight measurements were performed before and after the thermal treatment of each specimen of shells, the resulting mass loss being 3.6% (thermal treatment at 600 °C), 4.8% (700 °C) and 10.4% (800 °C). It should be noted that according to the chemical analysis, approximately 3% of the mass of the samples is represented only by the organic component.

Therefore, the loss of mass after 180 s of heat treatment exclusively due to the decomposition of calcite, at 600 °C, is less than 1%, increasing to about 2% at 700 °C and approx. 7% at 800 °C. The rather small loss of weight even at 800 °C, where the reaction rate is high, is due to the fact that the sample requires some time for heating from room temperature to calcite decomposition temperature, which must be extracted from the total time of thermal treatment (180 s).

Because the sample was introduced in the pre-heated oven, the surface of the exoskeletons heats up strongly and quickly, while the core remains colder for a while, which makes the carbonate decomposition to take place mostly at the surface. Thus, a core–shell type particle may form, just like a bread whose shell is more porous than the core.

The theoretical maximum mass loss is about 46%, approx. 43% representing the maximum mass loss only according to the reaction (4), the result being close to the value practically obtained—of about 41%. Thus, after only 180 s of heating, about 5% and 10% of $CaCO_3$, respectively, is decomposed at 700 °C and 800 °C, respectively.

The SEM images of the thermally treated samples are presented in Fig. 5. It can be noticed that at 600 °C the structure of the shell is not strongly modified (Fig. 5a—inset) as a result of the thermal treatment. However, longitudinal cracks (Fig. 5a—area A) can be observed in the plane of the exoskeleton. These are parallel to the edges of the

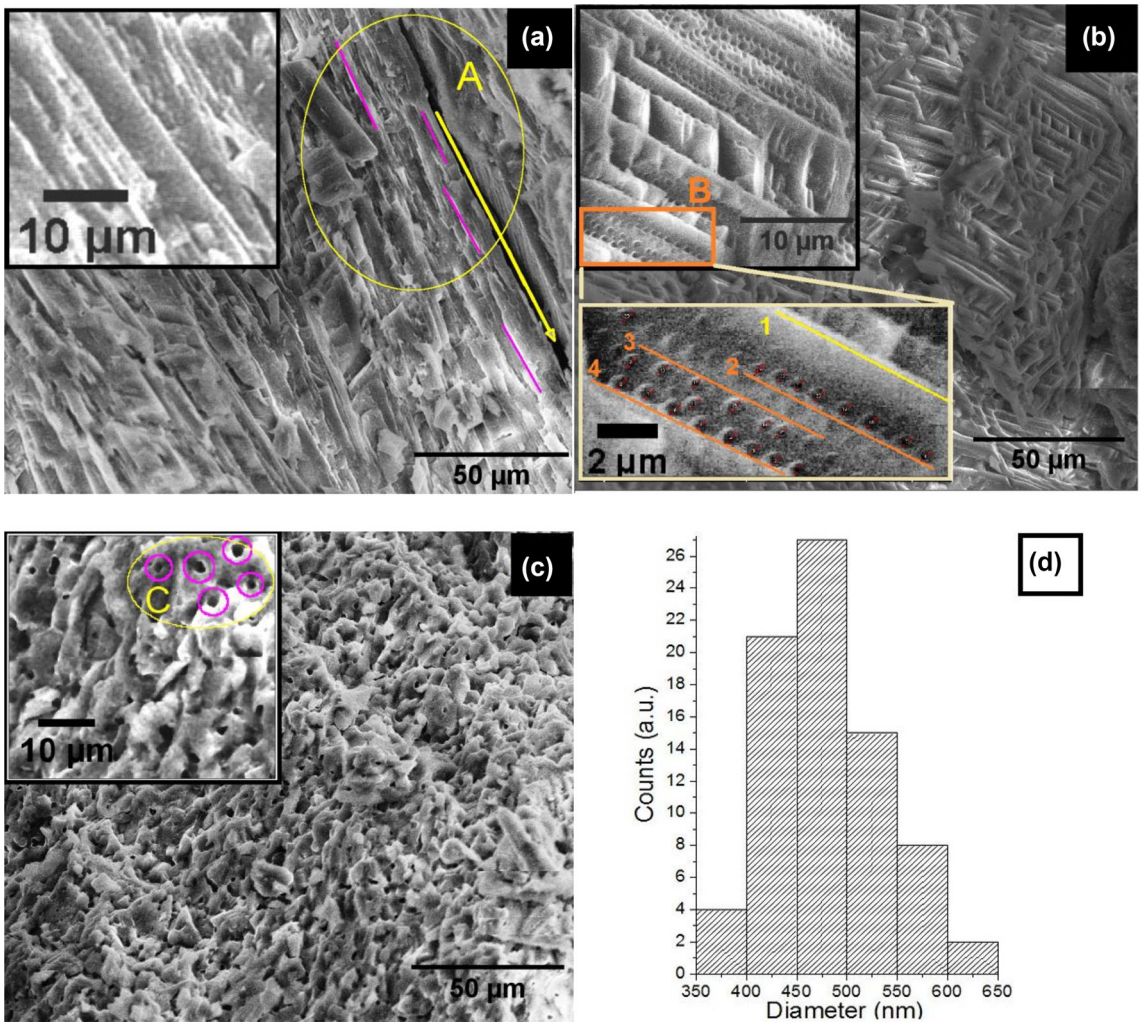

Fig. 5 SEM images of the exoskeletons thermally treated for 3 min; **a** MX600, **b** MX700, **c** MX800 and **d** histogram of voids for sample MX 700

calcite crystals, the structure having a higher resistance in the transverse direction on the surface of the exoskeleton than in the longitudinal direction after the heat treatment. At 700 °C equidistant perforations start to appear on all the exposed surfaces (inset in Fig. 5b), but the initial structure is preserved. These voids are collinear along straight lines parallel to the axes 2–4, and parallel to the edge of the crystal marked by axis 1. All the voids are circular, and a histogram (Fig. 5d) made for over 70 voids (some of them being visible in Fig. 5b inset, area B) shows a narrow dimensional distribution centered at 475 nm. The appearance of these collinear voids could be determined by biogenic nanometric channels placed transversely on the inorganic crystals (Schäffer et al. 1997), which allow the transfer of body fluids from the inside of the shells to the outside and the oriented growth of aragonite crystals from the exoskeleton. At 800 °C the lamellar structure characteristic for shells is destroyed and a porous and more friable structure with disordered voids can be observed (Fig. 5c—zone C), in agreement with literature mentioning that higher temperatures may alter the structure of the shell (Hou et al. 2016). The conclusion of this experiment is that 700 °C is a proper temperature for the texturing of this material. The perforations that create active centers for further potential chemical or physical interactions or the formed nanochannels can be used as a template for growing various large diameter nanotubes.

Conclusions

Mytilus galloprovincialis contain two crystalline polymorphs (aragonite, calcite) and present a well-defined and ordered inner structure, compared to *Mya arenaria* and *Cerastoderma edule* which contain the single crystalline phase aragonite. The growth of aragonite along the (012) plane differs strongly between the three species, *Cerastoderma edule* showing the strongest oriented growth among the studied species. We hypothesize that this major difference in the orientation of the crystalline growth of aragonite depending on the species can be an imprint for the recognition of some species after the analysis of some pieces of their exoskeletons. However, a thorough study of other environmental factors that may influence the particularly oriented growth of aragonite is needed. For MG type shells, the prismatic layer is surprisingly large in size, up to more than 80% of total thickness. The thermal transformation of aragonite starts at temperatures lower than 250 °C, but the transformation rate at this temperature is much higher in the case of *Cerastoderma edule* than in the case of the other two species. The weight percentage of $CaCO_3$ is above 96% for all the species. The thermal analysis indicates that the calcite decomposition starts at about 591 °C. The texturing of exoskeletons is achievable by heating them for only 180 s at 700 °C, where equidistant round perforations with diameters of a few hundreds of nanometers start to appear on all exposed surfaces, opening the possibility to use this material as, for example, consuming template for the synthesis of nanotubes from inorganic materials or in water purification tests as adsorbents of nitrate, phosphate and so on.

Acknowledgements This work was supported by a grant of the Romanian Ministry of Education and Research, CNCS—UEFISCDI, project number PN-III-P1-1.1-TE-2019-2116, within PNCDI III.

Data availability Electronic Raw Data associated with this article can be downloaded from https://data.mendeley.com/datasets/s8m6r6z4zy/1 https://doi.org/10.17632/s8m6r6z4zy.1.

Declarations

Conflict of interest The authors declare they have no conflicts of interest of any kind.

References

Abali M et al (2021) Removal of nitrate ions by adsorption onto microparticles of shrimp-shells waste: application to wastewater of infiltration-percolation process of the city of Agadir (Morocco). Mater Today Proc 37:3898–3904

Agbaje OBA, Dominguez JG, Jacob DE (2021) Organic biopolymers of venus clams: collagen-related matrix in the bivalve shells with crossed-lamellar ultrastructure. Biochem Biophys Rep 26:100939

An Y, Liu Z, Wenjian Wu (2013) Phase transition of aragonite in abalone nacre. Phase Transit 86(4):391–395

Aziz K et al (2023) A novel hydrogel beads based copper-doped cerastoderma edule shells@alginate biocomposite for highly fungicide sorption from aqueous medium. Chemosphere 311:136932

Barros MC, Bello PM, Bao M, Torrado JJ (2009) From waste to commodity: transforming shells into high purity calcium carbonate. J Clean Prod 17(3):400–407

Ben-Nissan B (2003) Natural bioceramics: from coral to bone and beyond. Curr Opin Solid State Mater Sci 7(4–5):283–288

Bragg WL, Langworthy FRS (1924) The structure of aragonite. Proc R Soc A 105:16–39

Bucur A et al (2022) Eco-valorification of marine shells by hydrothermal conversion in alkaline media. Dig J Nanomater Biostruct 17(1):153–160

Caspi EN, Pokroy B, Lee LP, Zolotoyabko E (2005) On the structure of aragonite. Acta Crystallogr B Struct Sci B 61:129–132

Connors MJ et al (2012) Three-dimensional structure of the shell plate assembly of the chiton tonicella marmorea and its biomechanical consequences. J Struct Biol 177(2):314–328. https://doi.org/10.1016/j.jsb.2011.12.019

Ehrlich H et al (2020) Conchixes: organic scaffolds which resemble the size and shapes of mollusks shells, their isolation and potential multifunctional applications. Appl Phys A Mater Sci Process 126(7):1–13. https://doi.org/10.1007/s00339-020-03728-7

Harayashiki CA, Yokota FM, Cariou E, Castro ÍB (2020) Mollusk shell alterations resulting from coastal contamination and other environmental factors. Environ Pollut 265:114881

Hart A (2020) Mini-review of waste shell-derived materials' applications. Waste Manag Res 38(5):514–527

Hou Y et al (2016) Marine shells: potential opportunities for extraction of functional and health-promoting materials. Crit Rev Environ Sci Technol 46(11–12):1047–1116

Ishizawa N, Setoguchi H, Yanagisawa K (2013) Structural evolution of calcite at high temperatures: phase V unveiled. Sci Rep 3:2832

Ismail R et al (2021) The potential use of green mussel (Perna Viridis) shells for synthetic calcium carbonate polymorphs in biomaterials. J Cryst Growth 572(July):126282. https://doi.org/10.1016/j.jcrysgro.2021.126282

Johnson CM (2013) Differential scanning calorimetry as a tool for protein folding and stability. Arch Biochem Biophys 531(1–2):100–109. https://doi.org/10.1016/j.abb.2012.09.008

Jones MI, Wang LY, Abeynaike A, Patterson DA (2011) Utilisation of waste material for environmental applications: calcination of mussel shells for waste water treatment. Adv Appl Ceram 110(5):280–286

Li H, Jin D, Li R, Li X (2015) Structural and mechanical characterization of thermally treated conch shells. J Miner Met Mater Soc (JOM) 67(4):720–725. https://doi.org/10.1007/s11837-015-1330-y

Li YY, Liang SM, Ji HM, Li XW (2022) Distinctive impact of heat treatment on the mechanical behavior of nacreous and crossed-lamellar structures in biological shells: critical role of organic matrix. ACS Biomater Sci Eng 8(3):1143–1155. https://doi.org/10.1021/acsbiomaterials.1c01538

Lin H et al (2022) Reutilization of waste oyster shell as filler for filter for drinking water pretreatment: feasibility and implication. J Environ Manag 315:115142

Marin F, Le Roy N, Marie B (2012) The formation and mineralization of mollusk shell. Front Biosci S4:1099–1125

Martínez-García C, González-Fonteboa B, Carro-López D, Pérez-Ordóñez JL (2020) Mussel shells: a canning industry by-product converted into a bio-based insulation material. J Clean Prod 269:122343

Momma K, Izumi F (2011) VESTA 3 for three-dimensional visualization of crystal, volumetric and morphology data. J Appl Crystallogr 44(6):1272–1276

Morris JP, Wang Y, Backeljau T, Chapelle G (2016) Biomimetic and bio-inspired uses of mollusc shells. Mar Genom 27(2016):85–90. https://doi.org/10.1016/j.margen.2016.04.001

Odeh M, Doscher C, Cochrane TA (2022) Removal of zinc from surface runoff by using recycled mussel shell waste as treatment media, with and without heat treatment. Environ Technol Innov 28:102814

Owuamanam S, Cree D (2020) Progress of bio-calcium carbonate waste eggshell and seashell fillers in polymer composites: a review. J Compos Sci 4(2):70

Pap S et al (2022) Enhanced phosphate removal and potential recovery from wastewater by thermo-chemically calcinated shell adsorbents. Sci Total Environ 814(152794):2022. https://doi.org/10.1016/j.scitotenv.2021.152794

Pokroy B, Fitch AN, Zolotoyabko E (2007) Structure of biogenic aragonite ($CaCO_3$). Cryst Growth Des 7(9):1580–1583

Rodríguez-Carvajal J (1993) Recent advances in magnetic structure determination by neutron powder diffraction. Phys B Phys Condensed Matter 192(1–2):55–69

Ruiz-Hitzky E, Darder M, Aranda P (2005) Functional biopolymer nanocomposites based on layered solids. J Mater Chem 15(35–36):3650–3662

Saruwatari K et al (2009) Nucleation and growth of aragonite crystals at the growth front of nacres in pearl oyster, Pinctada Fucata. Biomaterials 30(16):3028–3034. https://doi.org/10.1016/j.biomaterials.2009.03.011

Schäffer TE et al (1997) Does abalone nacre form by heteroepitaxial nucleation or by growth through mineral bridges? Chem Mater 9(8):1731–1740

Schneider CA, Rasband WS, Eliceiri KW (2012) NIH image to imageJ: 25 years of image analysis. Nat Methods 9(7):671–675. https://doi.org/10.1038/nmeth.2089

Shafiu A, Ismail M, Ibrahim TAT, Zakaria ZAB (2013) Synthesis and characterisation of calcium carbonate aragonite nanocrystals from cockle shell powder (Anadara Granosa). J Nanomaterials 2013:1–9

Silva TH et al (2019) The potential use of oyster shell waste in new value-added by-product. Resources 8(1):1–15

Simonet Roda M et al (2019) Calcite fibre formation in modern brachiopod shells. Sci Rep 9(598):1–15

Summa D et al (2022) Trends and opportunities of bivalve shells' waste valorization in a prospect of circular blue bioeconomy. Resources 11(5):1–16

Tran TT, Ngoc NTT, Shigeru S, Jhy CL (2021) Enhanced phosphate removal by thermally pretreated waste oyster shells. J Mater Cycles Waste Manag 23(1):177–185. https://doi.org/10.1007/s10163-020-01112-4

Troncoso OP et al (2020) Mechanical properties of calcite- and aragonite-based structures by nanoindentation tests. Bioinspir Biomim Nanobiomater 9(2):112–121

Von Ahnen M, Pedersen PB, Dalsgaard J (2018) Nitrate removal from aquaculture effluents using woodchip bioreactors improved by adding sulfur granules and crushed seashells. Water Sci Technol 77(9):2301–2310

Wan Mohammad WASBW et al (2017) A review on seashells ash as partial cement replacement. IOP Conf Ser Mater Sci Eng 271(1):012059

Wang X et al (2014) Aragonite shells are more ancient than calcite ones in bivalves: new evidence based on omics. Mol Biol Rep 41(11):7067–7071

Yoshioka S, Kitano Y (1985) Transformation of aragonite to calcite through heating. Geochem J 19:245–249. https://doi.org/10.1007/s11033-014-3620-9